THÈSE

En vue de l'obtention du

DOCTORAT DE L'UNIVERSITÉ FÉDÉRALE TOULOUSE MIDI-PYRÉNÉES

Délivré par :
l'école nationale de l'aviation civile (ENAC)

Présentée et soutenue le *jj/mm/aaaa* **par :**
Florian SANSOU

Titre de la thèse

JURY

Premier MEMBRE	Professeur des universités	Président du jury
Second MEMBRE	Ingénieur de recherche	Rapporteur
Troisième MEMBRE	Chargé de recherche	Examinateur
Quatrième MEMBRE	Maître de conférences	Co-directeur de thèse
Ciquième MEMBRE	Directeur de recherche	Directeur de thèse

École doctorale et spécialité :
EDSYS : Automatique 4200046
Unité de Recherche :
Ecole Nationale d'Aviation Civile
Directeur(s) de Thèse :
Premier DIRECTEUR et *Second DIRECTEUR*
Rapporteurs :
Premier RAPPORTEUR et *Second RAPPORTEUR*

Acknowledgments

A faire en dernier :-)

Contents

Liste des figures

List of Tables

Introduction

Convertible drones have the ability to take off or land vertically and fly like an airplane. They are promising architectures providing energy efficient flight capabilities for strong endurance, as compared with classical coplanar UAVs, like quadcopters. This high degree of autonomy is highly desirable in classic applications such as visual detection tasks (e.g. surveillance, aerial photography, etc.), but also for environmental exploration and physical interaction.

Chapter 1

Darko UAV modelling

1.1 Model of the DarkO UAV

The DarkO UAV, designed and developed at the Ecole Nationale de l'Aviation Civile (ENAC) in Toulouse (France), is a clear example of a convertible UAV with a so-called tail-sitter architecture. DarkO is assembled from multiple 3D printed Onyx parts (a highly robust material comprising omnidirectional carbon fibres). All surfaces are interlocked on a single axis, so that the drone can be easily disassembled for parts replacement or to gain access to the on-board electronics.

The on-board autopilot is an Apogee [1] board manufactured at ENAC, see Fig. 1.1. The autopilot provides the option of recording the on-board data on an SD

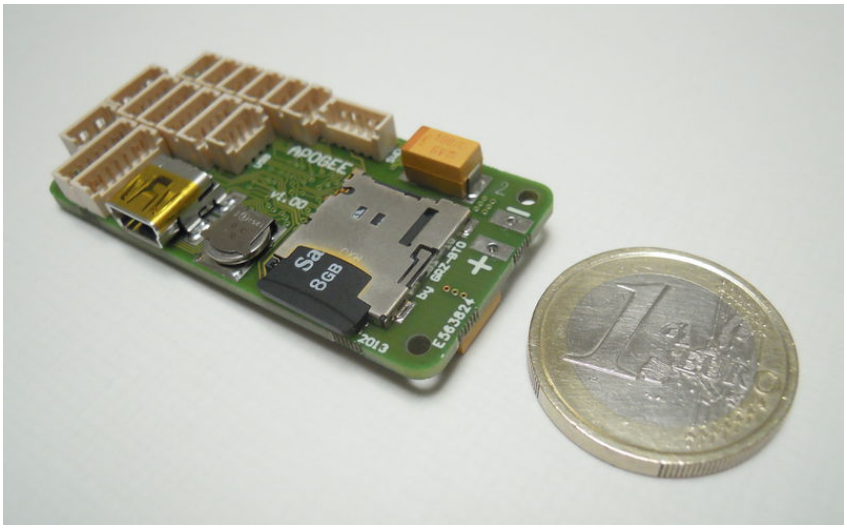

Figure 1.1: Apogee v1.00 top view.

memory card, at the control frequency of 500 Hz, thus allowing for effective post-processing of acquired data. The communication protocol used between the autopilot and the Electronic Speed Controllers (ESCs) is Dshot 600. The ESCs are AIKON AK32 35A flash with an AM32 firmware. The ground-to-board communication is performed via a bidirectional channel based on XBee-PRO S1 modules.

[1] https://wiki.paparazziuav.org/wiki/Apogee/v1.00

DarkO's actuators consist in two propellers (T-Motor T5147) symmetrically placed

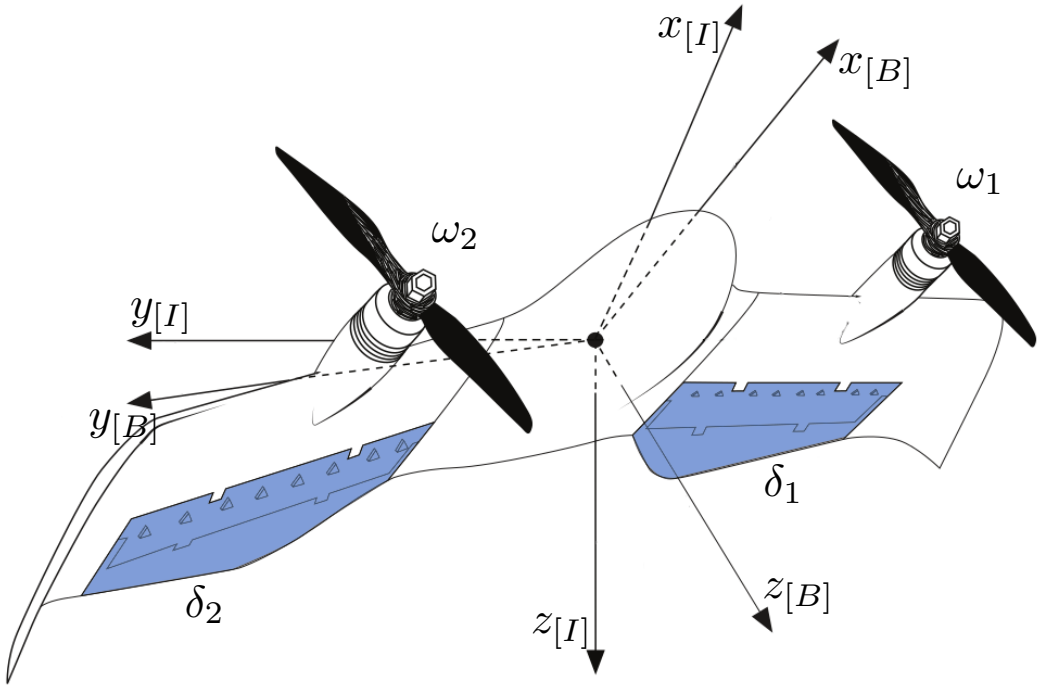

Figure 1.2: DarkO body frame with a schematic representation of the actuators.

at the front of the wing (shown in **black** in Fig. 1.2) powered by two T-Motor F30 2300kv electric motors and two elevons, placed at the back of the wing (shown in blue in Fig. 1.2) and acting as control surfaces. The elevons are driven by two MKS DS65K servomotors. Fig. 1.2 shows the DarkO model, together with a NED inertial reference frame (or world frame) "i" linked to the Earth's surface, and a body reference frame "b" attached to the drone, with x_b corresponding to the roll axis (the propellers axe laying in the $z_\mathrm{b} = 0$ plane), y_b the pitch axis (the direction of the wings), z_b the yaw axis. Using the same notation as in [Lustosa 2019], the left and right propeller/elevon are denoted by using subscripts $i = 1$ (left) and $i = 2$ (right). The sign convention will be defined positive for the elevons positions δ_1, δ_2 when they create a pitch-up moment with the propellers rotating in a opposite directions with angular speeds $\omega_1 > 0$ and $\omega_2 < 0$, respectively.

1.1.1 Full nonlinear model

Exploiting the modelling reported in [Lustosa 2019] and [Olszanecki Barth 2020], an accurate model of the DarkO dynamics describes the position $\boldsymbol{p} \in \mathbb{R}^3$ of the origin of the body frame and its velocity $\boldsymbol{v} = \dot{\boldsymbol{p}} \in \mathbb{R}^3$, in addition to its orientation, well

Parameter or coefficient	Value	Units
m (drone mass)	0.519	kg
b (wingspan)	0.542	m
c (aerodynamic cord)	0.13	m
$\boldsymbol{B} = \text{diag}(b, c, b)$	$\text{diag}(0.542, 0.13, 0.542)$	m
S (wing area)	0.026936	m^2
S_{wet} (wet area)	0.0180	m^2
S_{p} (propeller area)	0.0127	m^2
$\boldsymbol{J} = \text{diag}(J_x, J_y, J_z)$	$\text{diag}(0.0072, 0.0004, 0.0086)$	$\text{kg}\,\text{m}^2$
k_{f} (propeller thrust)	1.7800e-8	$\text{kg}\,\text{m}$
k_{m}(propeller torque)	2.1065e-10	$\text{kg}\,\text{m}^2$
p_x (propeller x location)	0.065	m
p_y (propeller y location)	0.162	m
a_y (lift y position)	0.1504	m
ξ_{f} (elevons lift)	0.2	–
ξ_{m} (elevons torque)	1.4	–
ρ (air density)	1.225	$\text{kg}\,\text{m}^{-3}$
C_{d} (drag coefficient)	0.1644	–
C_y (lateral coefficient)	0	–
C_ℓ (lift coefficient)	5.4001	–
Δ_{r} (UAV centering)	-0.0145	m

Table 1.1: Identified numerical parameters of the DarkO model.

represented by a quaternion $\boldsymbol{q} \in \mathbb{S}^3 := \{\boldsymbol{q} \in \mathbb{R}^4 : |\boldsymbol{q}| = 1\}$ and its angular velocity $\boldsymbol{\omega}_{\text{b}}$ represented in the body frame, which satisfies $\dot{\boldsymbol{q}} = \frac{1}{2}\boldsymbol{q} \otimes \left[\begin{smallmatrix} 0 \\ \boldsymbol{\omega}_{\text{b}} \end{smallmatrix}\right]$, where $\otimes$ denotes the quaternion product (see [Lustosa 2019, Olszanecki Barth 2020] or the tutorial [Hua 2013] for the details). Selecting the overall state as $\boldsymbol{x} := (\boldsymbol{p},\ \boldsymbol{v},\ \boldsymbol{q},\ \boldsymbol{\omega}_{\text{b}})$, the mathematical model derived in [Lustosa 2019], depend on a set of parameters listed in Table 1.1, where we also report the value obtained from a system identification [Sansou 2022]. The dynamic model can be written as

$$\begin{cases} m\dot{\boldsymbol{v}} = -m\boldsymbol{g} + \boldsymbol{R}(\boldsymbol{q})\boldsymbol{F}_{\text{b}}, & \text{(1.1a)} \\ \boldsymbol{J}\dot{\boldsymbol{\omega}}_{\text{b}} = -\left[\boldsymbol{\omega}_{\text{b}}\right]_\times \boldsymbol{J}\boldsymbol{\omega}_{\text{b}} + \boldsymbol{M}_{\text{b}}, & \text{(1.1b)} \end{cases}$$

where $\boldsymbol{g} := \left[\begin{smallmatrix} 0 & 0 & 9.81 \end{smallmatrix}\right]^\top$ denotes the gravity vector, $m \in \mathbb{R}$ is the mass, $\boldsymbol{J} \in \mathbb{R}^{3\times3}$ is the diagonal moment of inertia (see Table 1.1) and, partitioning the quaternion $\boldsymbol{q} \in \mathbb{S}^3$ as $\boldsymbol{q} := \left[\eta\ \boldsymbol{\epsilon}^\top\right]^\top$, the corresponding rotation matrix $\boldsymbol{R}(\boldsymbol{q}) \in SO(3) := \{\boldsymbol{R} \in \mathbb{R}^{3\times3} :\ \boldsymbol{R}^\top\boldsymbol{R} = \mathbb{I}_3, \det(\boldsymbol{R}) = 1\}$ is defined as (see [Hua 2013])

$$\boldsymbol{R}(\boldsymbol{q}) := \mathbb{I}_3 + 2\eta\left[\boldsymbol{\epsilon}\right]_\times + 2\left[\boldsymbol{\epsilon}\right]_\times^2. \tag{1.2}$$

According to [Lustosa 2019] the force and moment vectors $\boldsymbol{F}_\mathrm{b}$ and $\boldsymbol{M}_\mathrm{b}$ in (1.1) depend on (i) the state $\boldsymbol{x}$, (ii) the disturbance $\boldsymbol{w} \in \mathbb{R}^3$, representing the wind speed in the world frame, and (iii) the actuators commands (see Figure 1.2), comprising the two propellers' rotational speeds $\omega_1, \omega_2 \in \mathbb{R}$ and the two elevons' deflections $\delta_1, \delta_2 \in \mathbb{R}$. Let us first consider the actuators commands' effect. Each propeller generates a thrust $\boldsymbol{T}_i$ oriented in the x direction of the body frame and a moment $\boldsymbol{N}_i$ about the same axis:

$$\boldsymbol{T}_i := \begin{bmatrix} \tau_i \\ 0 \\ 0 \end{bmatrix} := \begin{bmatrix} k_\mathrm{f}\omega_i^2 \\ 0 \\ 0 \end{bmatrix}, \ \boldsymbol{N}_i := (-1)^i \frac{k_\mathrm{m}}{k_\mathrm{f}} \boldsymbol{T}_i, \quad i = 1, 2. \tag{1.3}$$

Each elevon's position $\delta_i \in \mathbb{R}$ is assigned by a servo-motor that imposes an efficiency level (in terms of airstream deflection) quantified by two skew-symmetric matrices:

$$\boldsymbol{\Delta}_i^\mathrm{f} := \begin{bmatrix} 0 & 0 & \xi_\mathrm{f}\delta_i \\ 0 & 0 & 0 \\ -\xi_\mathrm{f}\delta_i & 0 & 0 \end{bmatrix}, \ \boldsymbol{\Delta}_i^\mathrm{m} := \begin{bmatrix} 0 & 0 & \xi_\mathrm{m}\delta_i \\ 0 & 0 & 0 \\ -\xi_\mathrm{m}\delta_i & 0 & 0 \end{bmatrix}, \tag{1.4}$$

$i = 1, 2$. The constant parameters k_f, k_m, ξ_f, ξ_m appearing in (1.3) and (1.4) are listed in Table 1.1.

With the above actuation quantities, we may rearrange the dynamics given in [Lustosa 2019, eqns (97), (98)] (see also [Sansou 2022]) and express $\boldsymbol{F}_\mathrm{b}$ and $\boldsymbol{M}_\mathrm{b}$ in (1.1) as

$$\begin{aligned} \boldsymbol{F}_\mathrm{b} := \boldsymbol{T}_1 + \boldsymbol{T}_2 &+ \frac{S_\mathrm{wet}}{4S_\mathrm{p}} \boldsymbol{\Phi}^{(\mathrm{fv})} \Big((\boldsymbol{\Delta}_1^\mathrm{f} - \mathbb{I}_3)\boldsymbol{T}_1 + (\boldsymbol{\Delta}_2^\mathrm{f} - \mathbb{I}_3)\boldsymbol{T}_2 \Big) \\ &+ \frac{1}{4}\rho S \boldsymbol{\Phi}^{(\mathrm{fv})} \Big(\boldsymbol{\Delta}_1^\mathrm{f} + \boldsymbol{\Delta}_2^\mathrm{f} - 2\mathbb{I}_3 \Big) \|\boldsymbol{v}_\mathrm{b}\| \boldsymbol{v}_\mathrm{b} \\ &+ \frac{1}{4}\rho S \boldsymbol{\Phi}^{(\mathrm{mv})} \Big(\boldsymbol{\Delta}_1^\mathrm{f} + \boldsymbol{\Delta}_2^\mathrm{f} - 2\mathbb{I}_3 \Big) \boldsymbol{B} \|\boldsymbol{v}_\mathrm{b}\| \boldsymbol{\omega}_\mathrm{b}, \end{aligned} \tag{1.5}$$

$$
\begin{aligned}
\boldsymbol{M}_{\mathrm{b}} :=\ & \boldsymbol{N}_1 + \boldsymbol{N}_2 + \begin{bmatrix} p_x \\ p_y \\ 0 \end{bmatrix}_{\times} \boldsymbol{T}_1 + \begin{bmatrix} p_x \\ -p_y \\ 0 \end{bmatrix}_{\times} \boldsymbol{T}_2 \\
& - \frac{S_{\mathrm{wet}}}{4S_{\mathrm{p}}} \Big(\boldsymbol{B}\boldsymbol{\Phi}^{(\mathrm{mv})} (\boldsymbol{\Delta}_1^{\mathrm{m}} - \mathbb{I}_3) + \begin{bmatrix} 0 \\ a_y \\ 0 \end{bmatrix}_{\times} \boldsymbol{\Phi}^{(\mathrm{fv})} (\boldsymbol{\Delta}_1^{\mathrm{m}} + \mathbb{I}_3) \Big) \boldsymbol{T}_1 \\
& - \frac{S_{\mathrm{wet}}}{4S_{\mathrm{p}}} \Big(\boldsymbol{B}\boldsymbol{\Phi}^{(\mathrm{mv})} (\boldsymbol{\Delta}_2^{\mathrm{m}} - \mathbb{I}_3) + \begin{bmatrix} 0 \\ -a_y \\ 0 \end{bmatrix}_{\times} \boldsymbol{\Phi}^{(\mathrm{fv})} (\boldsymbol{\Delta}_2^{\mathrm{m}} + \mathbb{I}_3) \Big) \boldsymbol{T}_2 \\
& + \frac{1}{4}\rho S \Big(\Big(\begin{bmatrix} 0 \\ a_y \\ 0 \end{bmatrix}_{\times} \boldsymbol{\Phi}^{(\mathrm{fv})} + \boldsymbol{B}\boldsymbol{\Phi}^{(\mathrm{mv})} \Big) \boldsymbol{\Delta}_1^{\mathrm{m}} \\
& + \Big(\begin{bmatrix} 0 \\ -a_y \\ 0 \end{bmatrix}_{\times} \boldsymbol{\Phi}^{(\mathrm{fv})} + \boldsymbol{B}\boldsymbol{\Phi}^{(\mathrm{mv})} \Big) \boldsymbol{\Delta}_2^{\mathrm{m}} - 2\boldsymbol{B}\boldsymbol{\Phi}^{(\mathrm{mv})} \Big) \|\boldsymbol{v}_{\mathrm{b}}\| \boldsymbol{v}_{\mathrm{b}} \\
& + \frac{1}{4}\rho S \Big(\Big(\begin{bmatrix} 0 \\ a_y \\ 0 \end{bmatrix}_{\times} \boldsymbol{\Phi}^{(\mathrm{mv})} + \boldsymbol{B}\boldsymbol{\Phi}^{(\mathrm{m}\omega)} \Big) \boldsymbol{\Delta}_1^{\mathrm{m}} \\
& + \Big(\begin{bmatrix} 0 \\ -a_y \\ 0 \end{bmatrix}_{\times} \boldsymbol{\Phi}^{(\mathrm{mv})} + \boldsymbol{B}\boldsymbol{\Phi}^{(\mathrm{m}\omega)} \Big) \boldsymbol{\Delta}_2^{\mathrm{m}} - 2\boldsymbol{B}\boldsymbol{\Phi}^{(\mathrm{m}\omega)} \Big) \boldsymbol{B} \|\boldsymbol{v}_{\mathrm{b}}\| \boldsymbol{\omega}_{\mathrm{b}},
\end{aligned}
\tag{1.6}
$$

where $\boldsymbol{v}_{\mathrm{b}} := \boldsymbol{R}^{\top}(\boldsymbol{q})(\boldsymbol{v} - \boldsymbol{w})$ represents the air speed seen by the drone, represented in the body frame. In [Lustosa 2019], the scalars $\|\boldsymbol{v}_{\mathrm{b}}\|$ appearing in the expressions of $\boldsymbol{F}_{\mathrm{b}}$ and $\boldsymbol{M}_{\mathrm{b}}$ are replaced by the scalar $\eta = \sqrt{\|\boldsymbol{v}_{\mathrm{b}}\|^2 + \mu c^2 \|\boldsymbol{\omega}_{\mathrm{b}}\|^2}$, with $\mu \in \mathbb{R}$ being a parameter related to the model identification, but in the case of DarkO [Sansou 2022], the identification provides $\mu = 0$, therefore we present a simplified description here. The constant aerodynamic coefficients' matrix $\boldsymbol{\Phi} := \begin{bmatrix} \boldsymbol{\Phi}^{(\mathrm{fv})} & \boldsymbol{\Phi}^{(\mathrm{mv})\top} \\ \boldsymbol{\Phi}^{(\mathrm{mv})} & \boldsymbol{\Phi}^{(\mathrm{m}\omega)} \end{bmatrix} \in \mathbb{R}^{6\times 6}$, is defined in [Olszanecki Barth 2020, eqs. (6)–(9)] as $\boldsymbol{\Phi}^{(\mathrm{fv})} := \mathrm{diag}(C_{\mathrm{d}}, C_y, C_\ell)$ and

$$
\left[\begin{array}{c|c} \boldsymbol{\Phi}^{(\mathrm{mv})} & \boldsymbol{\Phi}^{(\mathrm{m}\omega)} \end{array}\right] :=
\left[\begin{array}{ccc|ccc}
0 & 0 & 0 & 0.1396 & 0 & 0.0573 \\
0 & 0 & -\frac{\Delta_{\mathrm{r}}}{c} C_\ell & 0 & 0.6358 & 0 \\
0 & 0 & 0 & 0.0405 & 0 & 0.0019
\end{array}\right],
$$

the numerical values of the constants being reported in Table 1.1 (these numerical values were not reported in [Lustosa 2019] and [Olszanecki Barth 2020] and are given here to allow reproducing our simulation results). The numerical values in Table 1.1 have been obtained by a model identification campaign [Sansou 2022]. In particuler, coefficient k_{f} was identified from the equation (1.3), which links the motor rotation speed ω_i with the generated traction, the minimum and maximum rotation speed and the time constant of the motor actuation chain. The diagonal elemnts of the inertia $\boldsymbol{J}$ were measured using a bifilar pendulum system. This method is widely used in the drone field [Jardin 2012], and is based on the period

of oscillation about each one of the three axes (x_b,y_b,z_b) of the drone suspended by two wires, which forms a torsion pendulum as shown in Fig. 1.4. It is interesting to note that the surface area blown by the propellers represents 67 percent of the drone's total surface area.

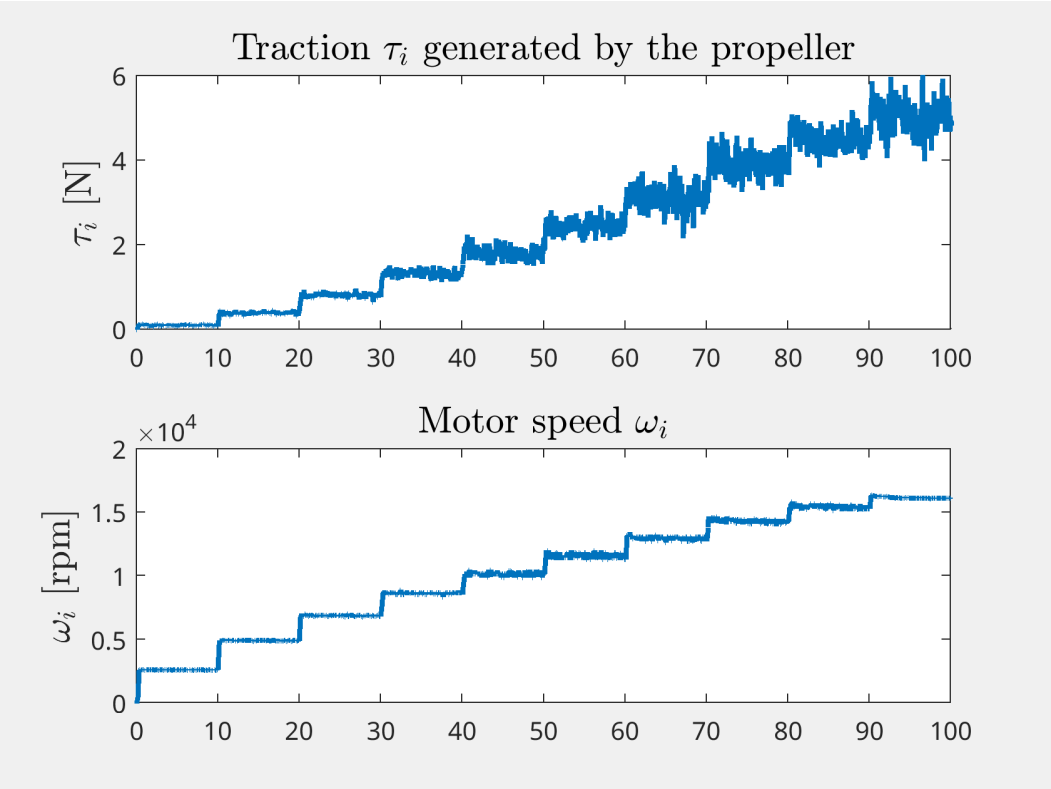

Figure 1.3: Input-output response of an Esc-Motor-Propeller assembly.

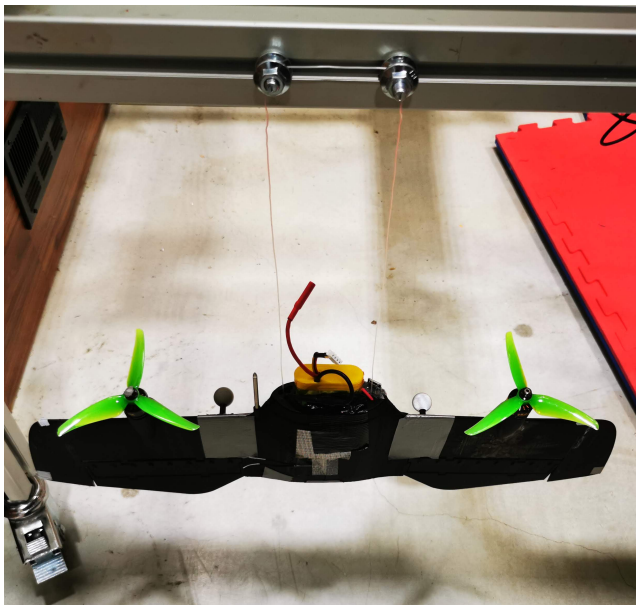

Figure 1.4: Bifilar pendulum mounting for the identication of $\boldsymbol{J}$.

Chapter 2

Chapitre2

Contents

2.1 section1

2.1.1 subsection1a

Chapter 3

Chapitre2

3.1 section1

3.1.1 subsection1a

Conclusion

Ce manuscrit de thèse rapporte

Appendix A

Exemple d'annexe

A.1 Exemple d'annexe

Bibliography

[Hua 2013] Hua, M.-D., Hamel, T., Morin, P. and Samson, C. *Introduction to feedback control of underactuated VTOL vehicles: A review of basic control design ideas and principles.* IEEE, Control Systems, vol. 33, pages 61–75, 02 2013. [Online]. Available: http://dx.doi.org/10.1109/MCS.2012.2225931. (Cited in page 5.)

[Jardin 2012] Jardin, M. and Mueller, E. *Optimized Measurements of UAV Mass Moment of Inertia with a Bifilar Pendulum.* In AIAA Guidance, Navigation and Control Conference and Exhibit, 2012. (Cited in page 7.)

[Lustosa 2019] Lustosa, L. R., Defaÿ, F. and Moschetta, J.-M. *Global Singularity-Free Aerodynamic Model for Algorithmic Flight Control of Tail Sitters.* Journal of Guidance, Control, and Dynamics, vol. 42, no. 2, pages 303–316, February 2019. [Online]. Available: http://dx.doi.org/10.2514/1.G003374. (Cited in pages 4, 5, 6, and 7.)

[Olszanecki Barth 2020] Olszanecki Barth, J. M., Condomines, J.-P., Bronz, M., Moschetta, J.-M., Join, C. and Fliess, M. *Model-free control algorithms for micro air vehicles with transitioning flight capabilities.* International Journal of Micro Air Vehicles, vol. 12, pages 1–22, April 2020. [Online]. Available: http://dx.doi.org/10.1177/1756829320914264. (Cited in pages 4, 5, and 7.)

[Sansou 2022] Sansou, F. *Commande hybride d'un drone convertible pour des déplacements sous optimaux.* Master Thesis. ENAC Toulouse, 2022. [Online]. Available: http://dx.doi.org/10.48550/ARXIV.2203.15387. (Cited in pages 5, 6, and 7.)

Résumé : resume
Mots clés : mots, clefs

Abstract: abstrat
Keywords: key, words